buildings

MDPI

Article

Probabilistic Risk-Based Performance Evaluation of Seismically Base-Isolated Steel Structures Subjected to Far-Field Earthquakes

Aryan Rezaei Rad [1,*] and Mehdi Banazadeh [2]

[1] Laboratory of Timber Construction (IBOIS), École Polytechnique Fédérale de Lausanne (EPFL), CH-1015 Lausanne, Switzerland

[2] School of Civil and Environmental Engineering, Amirkabir University of Technology (Tehran Polytechnic), 15875-4413 Tehran, Iran; mbanazadeh@aut.ac.ir

* Correspondence: aryan.Rezaeirad@epfl.ch; Tel.: +41-21-69-34556

Received: 10 August 2018; Accepted: 12 September 2018; Published: 13 September 2018

Abstract: The performance of base-isolated steel structures having special moment frames is assessed. The archetypes, which are designed per ASCE/SEI 7–2016, are simulated in the Finite Element (FE) computational platform, OpenSees. Adopting nonlinear dynamic analyses using far-field ground motions, the performance of Drift-Sensitive Structural Components (DS-SC), and Drift-/Acceleration-Sensitive Non-Structural Components (DS/AS NSC) at slight, moderate, extensive, and collapse damage states are investigated. The effects of structural height, effective transformed period (T_{eff}), response modification coefficient (R_I), and isolation type on the performance of 26 archetypes mounted on Lead Rubber Bearings (LRBs) and Triple Concave Friction Pendulums (TCFPs) are evaluated. Computing 50-year probability of exceedance using the fragility curves and seismic hazard curves of the site, increasing T_{eff} reduces the role of R_I in the structural performance; variations in the height, as well as R_I, do not affect the risk of damages to the AS-NSC; the risk of collapse is not sensitive to the variations of T_{eff}. The TCFP systems represent superior performance than LRB systems in lower intensities. For longer periods and taller structures, the isolation type has less effect on the performance of NSC. Finally, the archetypes have less than 1% risk of collapse in 50 years; nevertheless, high-rise structures with R_I = 2.0 have more than 10% probability of collapse given the maximum earthquake.

Keywords: seismic isolation technology; lead rubber bearing (LRB); triple friction concave pendulum (TCFP); performance-based earthquake engineering; risk analysis; far-field ground motions; steel structures; special moment frames

1. Introduction

Isolation technology is considered as an effective seismic protective system in the field of earthquake engineering. Having a low horizontal stiffness and high compression modulus [1], isolation devices change the dynamic properties of structural systems. Transforming the frequency content of the input energy, isolation devices dissipate ground motion intensities and mitigate damages to superstructural components [1–3]. Generally, isolation systems are characterized in two main groups, namely elastomeric bearings and frictional bearings. Among elastomeric devices, Lead Rubber Bearings (LRBs) are one of the commonly used isolators. They are made out of layers of steel plates, which control vertical stiffness, bounded with natural rubbers together with a lead plug, which governs initial stiffness and the damping content (Figure 1a). Figure 1b shows a typical hysteresis response of LRBs, where a hardening behavior at large deformations is observed [4]. Among

Frictional Pendulum Systems (FPSs), Triple Concave Friction Pendulum (TCFP) bearings [5], which are studied in the present paper, have been recently introduced. TCFPs consist of four concave surfaces and provide three independent sliding elements [6] (Figure 2a). A TCFP isolator has five regimes of movement, representing an adaptive behavior based on the ground motion intensity [7,8] (Figure 2b). The geometry of the concave surfaces can be designed in a way that provides an optimal stiffness and damping content and meets the performance targets [9]. These devices have demonstrated promising performance under seismic events [10], and consequently, new materials, such as shape memory alloys (SMA), are proposed to make such devices optimized [11]. As such, it is shown that SMA-LRB devices are more recoverable [12].

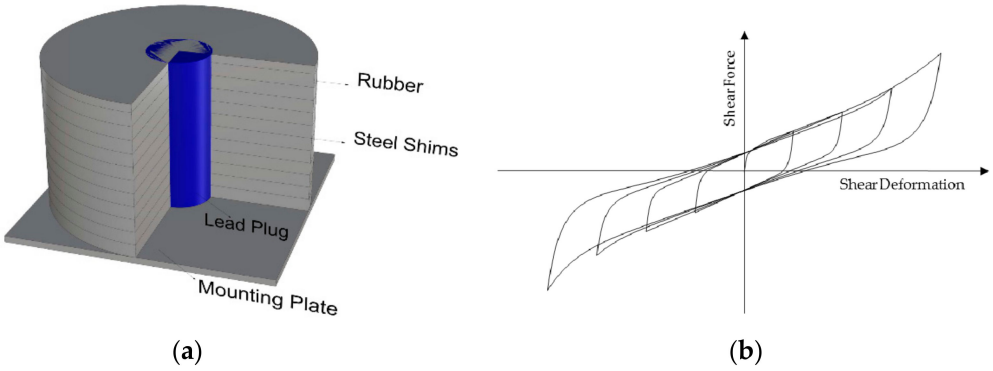

Figure 1. Schematic description of (**a**) a Lead Rubber Bearing (LRB) device (**b**) LRB nonlinear hysteresis behavior.

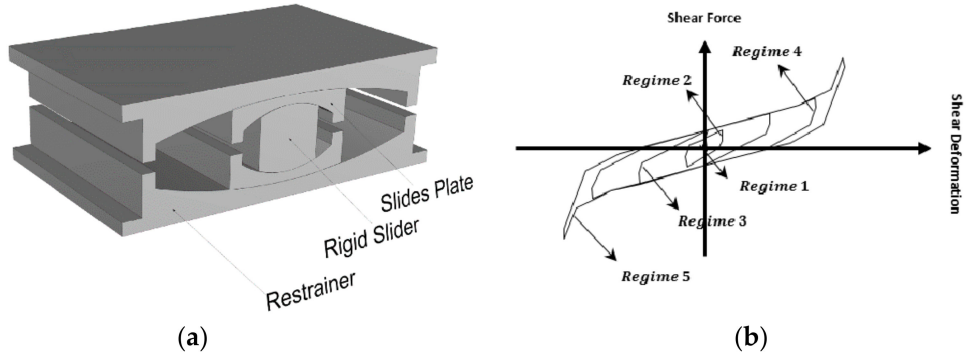

Figure 2. Schematic description of (**a**) a one-dimensional Triple Concave Friction Pendulum (TCFP) device (**b**) TCFP nonlinear hysteresis behavior [5].

Multiple building standards have provided guidelines to design isolated structures. Yenidogan and Erdik [13] provided an overview of the existing design process, where the influence of uncertainty sources is investigated. One of the well-known strategies to take uncertainties into account is the Performance-Based Earthquake Engineering (PBEE) methodology. The strategy includes a probabilistic relationship between the seismic demand and the structural capacity. Multiple sources of uncertainties such as modeling, design, and record-to-record (RTR) uncertainty can be taken into the account [14]. Using the fragility function concept, the framework has been implemented in several studies to evaluate the performance of seismically isolated structures. PBEE is applied to compare the performance of isolated and non-isolated bridges [15–17] and propose an optimal design strategy [18]. It appears that modeling uncertainty associated with isolation mechanical properties, as well as RTR variabilities affect the structural performance [15,16]. The performance of isolated and non-isolated buildings using PBEE have been widely compared as well [3,19]. Studies demonstrate that isolated systems decrease the response dispersion [3,20]. Furthermore, seismic reliability-based design methodology was investigated by Morgan and Mahin [21] and Castaldo et al. [22] to draw a possible improvement toward the design methodology and performance of structural systems isolated with friction pendulums.

Recently, risk evaluation methods have been applied in isolation technology through incorporating the multi-objective performance classification and integrating the business interruption concepts using the Federal Emergency management Agency, FEMA P−58 methodology [23]. Lee et al. [24] demonstrated the influence of isolation technique in reducing the damage costs. Banazadeh et al. [25,26] studied the risk-based cost-benefit analysis of seismically isolated structures equipped with viscous dampers. Also, Han et al. [27] investigated the risk analyses of non-ductile reinforced concrete buildings retrofitted with LRBs under mainshock-aftershock sequences. The results demonstrated that isolation retrofitting can decrease the risk of damage to building components, especially in higher stages. Furthermore, Cutfield et al. [28] conducted a life cycle analysis to compare the performance of a conventional and base-isolated steel braced structure. Recently, Tajammolian et al. [29] implemented the PBEE framework into the design investigation of TCFP isolated asymmetric structures, where the spectral acceleration reduces up to 20% in building damages using TCFPs.

Recently, resilience-based earthquake design framework has attracted attention. The methodology is a holistic framework to enhance the ability of a community to recover itself soon after a disaster. Some quantitative criteria have provided by Resilience-based Earthquake Design Initiative Rating System (REDi™) [30] where loss assessment, ambient resilience, organizational resilience, and building resilience are taken into the account. Regarding the isolation technology, it is close to reality to achieve far greater resilience at minimal additional investment. Notwithstanding that the recent design standards consider risk-targeted approach in their design methodology [31,32], the effect of influential design parameters on the performance of codified seismically base-isolated structures has not been addressed yet. Importantly, not only should a performance evaluation methodology assess structural components but also non-structural elements, which is the explicit target of a resilience-based design framework. The design concept lying behind the standard should be further examined to weigh the pros and cons of the code-intended performance objectives. This can significantly help the framework to integrate multi-disciplinary design and contingency planning into the PBEE and facilitate post-earthquake recovery.

In particular, the present study investigates the effect of following influential parameters on the probabilistic performance of steel moment resisting base-isolated structures: structural height (low-, mid-, and high-rise), fundamental periods of an isolated system (T_D, T_M) (ranging from 2.0 to 4.0 s), structural response modification numerical coefficient (R_I) (ranging from 1.0 to 2.0), and type of the isolators (LRBs and TCFPs). The effect of damping on the structural performance, which is another influential design factor [33], is beyond the scope of this paper. The archetypes are designed per the latest version of the ASCE standard, the ASCE/SEI 7-2016 [32]. For the performance assessment, nonlinear Incremental Dynamic Analysis (IDA) [34] using far-field ground motions listed in FEMA P695 [35] are applied. The limit state criteria for the slight, moderate, extensive, and collapse Damage State (DS) are compliant with the HAZUS-MH-MR4 [36]. The fragility curves and the 50-year probability of exceedance, which is computed by integrating each fragility curve over the site hazard curve, are compared in different DSs for (non-)structural components.

2. Development of Archetype Models

2.1. Design Strategy

It is assumed that the archetypes are located in the San Diego region, California, USA (32.715° N, 117.1625° W). The site class, risk category, and seismic design category of archetypes, required by the standard, are considered as "D", "3", and "D", respectively. The soil type can considerably affect the seismic response [37]. As such, using United States Geological Survey, USGS urban hazard maps [38], Type C is used as the soil category in the design process. The transformed design periods (T_D, and T_M)

(see Equation (1)), the response modification numerical coefficient (R_I), and structural height control the design workflow.

$$T_{eff} = 2\pi\sqrt{\frac{W}{K_{eff}g}} \quad (1)$$

where "g" is the gravity acceleration, "W" is the effective seismic weight, and K_{eff} is the effective stiffness of the isolated system at D_{eff} (K_M is the stiffness at maximum displacement, D_M and K_D is the stiffness at design displacement, D_D). Also, D_{eff} is calculated following Equation (2).

$$D_{eff} = \frac{gS_{eff-1}T_{eff}}{4\pi^2 B_{eff}} \quad (2)$$

where for maximum earthquakes, $S_{eff\text{-}1}$ is S_{M1} and for design earthquakes is S_{D1}. S_{M1} is MCE_R 5% damped spectral acceleration parameter at the 1-s period and S_{D1} is 2/3 S_{M1}. Also, B_{eff} is a numerical coefficient for the effective damping of the system, β_{eff}, at the displacement D_{eff}.

The amount of equivalent viscous damping of the isolation system, ξ_{eff} (see Equation (3)), at the design and maximum displacements depends on the mechanical properties of the production used by manufacturers. The mechanical details for LRBs are obtained from the production of the Bridgestone Corporation catalog [39]. The catalog is also providing the equivalent viscous damping corresponding to the design shear strain, which is 22% for 100% shear strain [39].

$$\xi_{eff} = \frac{1}{2\pi}\left[\frac{E_{loop}}{K_{eff}\,D_{eff}{}^2}\right] \quad (3)$$

where K_{eff} and D_{eff} are the effective stiffness and displacement, respectively, which represents the K_D or K_M, and E_{Loop} indicates the energy dissipated in each cycle of the hysteresis loop. Calculating ξ_{eff}, the damping factor, B_{eff}, is computed in accordance with table 14.5-1 of ASCE/SEI 7-2016 standard. Using the linear interpolation, as proposed by the standard, B_{eff} is 1.54 for ξ_{eff} = 22%.

The isolation design is an iterative trial and error process [40]. In order to select an appropriate transformed period, FEMA P750 [41], and FEMA P1050 [40] suggests that T_D and T_M should lie in the range of 2.0 to 4.0 s. Also, T_D is typically 15–25% less than T_M [42]. Therefore, the primitive values of the effective period lie in the range of 2.0 to 4.5 s. Furthermore, the R_I used to calculate the design forces in the building components from the elastic force demand should range from 1.0 to 2.0 per the ASCE standard, where following R_I values are assumed; R_I = 1.0, 1.5, 2.0. Dividing the building height into the low-rise, mid-rise, and high-rise systems per HAZUS MH-MR4 [36], 2-story, 4-story, 6-story, 8-story, and 10-story structures are considered. Totally, 22 archetypes mounted on LRB devices are designed (Table 1). Referring to the results which demonstrate that the mid-rise and high-rise LRB isolated structures with greater R_I are more vulnerable than the rest, two mid-rise (4-story) and two high-rise (8-story) archetypes mounted on TCFP isolators are designed (Table 1). Considering the design response spectrum, designing these two typical heights seems rational since the fundamental non-isolated period of 4- and 8-story buildings per ASCE/SEI 7-2016 lies in a part of the design spectrum which induces the greatest amount of acceleration.

Finally, through setting the same amount of ξ_{eff} and T_D between TCFP isolated archetypes and their peers (LRB isolated archetypes) at the design displacement, the same amount of K_D and T_D are derived, resulting in a same design force per ASCE/SEI 7-2016 section 17. As an advantage, each pair of LRB/TCFP isolated structures has the same superstructural section size. Nevertheless, the performance of TCFP isolated systems varies at the Maximum Considered Earthquake (MCE) level and other seismic intensities. The force-deformation response of the TCFP and LRB devices used in the archetypes #10 and #24 is illustrated in Figure 3 as an example. The isolators have similar K_D and ξ_{eff} at the displacements corresponding to the Design Basis Earthquake (DBE) level (0.25 m), but different KM and ξ_{eff} at the displacements associated with the MCE level (0.43 m).

Table 1. Archetypes.

ID	Floor	R_I	T_D (s)	T_M (s)	Sa-$_{TM}$ (g)	Isolator	ID	Floor	R_I	T_D (s)	T_M (s)	Sa-$_{TM}$ (g)	Isolator
1	2	1	2.0	2.2	0.32	LRB	14	6	2	3.0	3.3	0.21	LRB
2	2	2	2.0	2.2	0.32	LRB	15	6	1	3.0	3.3	0.21	LRB
3	4	1	2.0	2.25	0.32	LRB	16	6	1.5	3.0	3.3	0.21	LRB
4	4	1.5	2.0	2.25	0.32	LRB	17	8	2	3.0	3.3	0.21	LRB
5	4	2	2.0	2.25	0.32	LRB	18	8	1	4.0	4.3	0.16	LRB
6	4	1	2.5	2.7	0.26	LRB	19	8	1.5	4.0	4.3	0.16	LRB
7	4	2	2.5	2.7	0.26	LRB	20	8	2	4.0	4.3	0.16	LRB
8	4	1	3.0	3.3	0.21	LRB	21	10	1	4.0	4.3	0.16	LRB
9	4	1.5	3.0	3.3	0.21	LRB	22	10	2	4.0	4.3	0.16	LRB
10	4	2	3.0	3.3	0.21	LRB	23	4	2	2.0	2.25	0.32	TCFP
11	6	1	2.5	2.7	0.26	LRB	24	4	2	3.0	3.3	0.21	TCFP
12	6	2	2.5	2.7	0.26	LRB	25	8	2	3.0	3.3	0.21	TCFP
13	6	1	3.0	3.3	0.21	LRB	26	8	2	4.0	4.3	0.16	TCFP

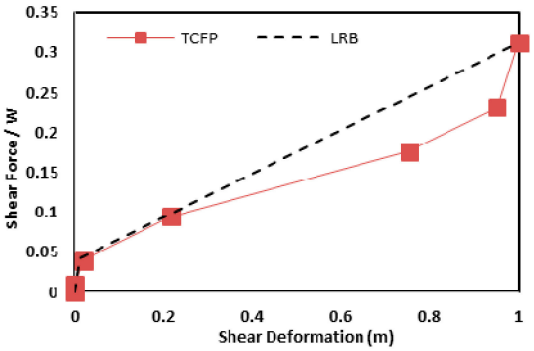

Figure 3. Backbone curve of the LRB model (model #10) and TCFP model (model #24).

2.2. Structural Design of Elements

Perimeter Special Moment Frames (SMFs) with steel type of ASTM A-36 were designed per the ASCE/SEI 7-2016 [32], ANSI/AISC 360-10 [43], and ANSI/AISC 341-10 [44]. Although the corner columns were under higher demand due to bidirectional seismic forces, the isolators reduced the imposed forces to the superstructure. As such, the SMFs were continuous along the perimeter. The non-perimeter frames were used only to carry the gravity loads. Wide flange sections and box sections were designed for the beams and columns, respectively. The dimension of the box elements was rectangular and ranges from 200 × 200 mm to 500 × 500 mm having 3.0 mm thickness. The dimension of the W-sections was selected from the American Institute of Steel Construction, AISC steel section database [45] and ranges from W10X19 to W12X30 for the gravity frames and W12X30 to W27X102 for SMFs. In Figure 4, the typical plan view of the archetypes, and 3D perspective view of a 4-story isolated structure are illustrated.

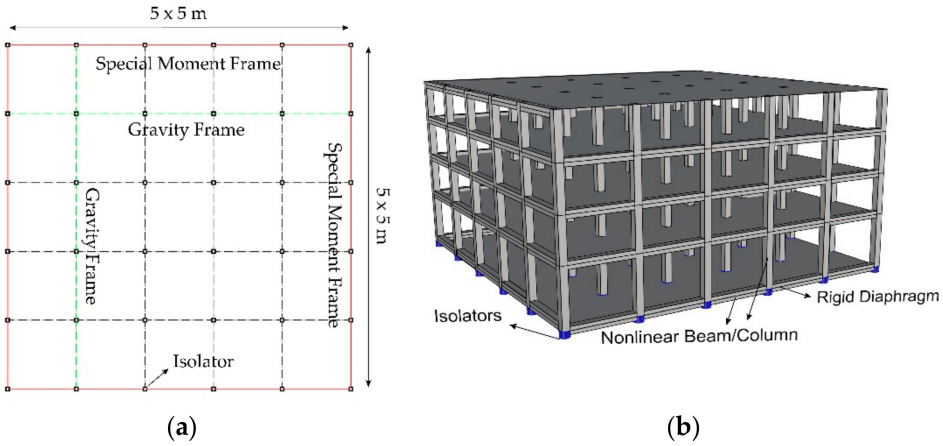

Figure 4. (**a**) Typical plan of the archetypes, (**b**) 3D view of 4-story isolated structures.

ASCE/SEI 7-2016 [32] specifies two main criteria for seismic isolator capabilities: (a) basic functionality requirements to maintain the functionality of building facilities immediately after the DBE level, and (b) target reliability which implicitly limits the failure probability of structural stability to 2.5% for primary structural components. To comply with the requirements, the bearings size selection and adequate assessment of isolators in service loads, DBE level, and MCE level Load and Resistance Factor Design (LRFD) method in the analysis and design of isolations, introduced by Constantinou et al. [46] was applied. Furthermore, the simplified design method to calculate the K_{eff} and E_{Loop} of the TCFP devices [6] was used. Table 2 provides the mechanical properties of the LRB devices and the geometric and frictional parameters used to design the TCFP bearings.

Table 2. LRB and TCFP mechanical and geometrical properties.

LRB Devices [39]		TCFP Devices [2]	
Property	**Value**	**Property**	**Value**
Rubber Shear Modulus	0.385 N/mm^2 (for γ = 100%)	Friction Coefficient (μ_1)	0.01
Young's Modulus	2.2 N/mm^2	Friction Coefficient (μ_2)	0.04
Apparent Shear Modulus of Lead	0.583 N/mm^2	Friction Coefficient (μ_3)	0.1
Shear Stress at Yield of Lead	7.967 N/mm^2	Displacement Limit (d_1)	0.05 m
Rubber Elongation at Break	600 (%)	Displacement Limit (d_2)	0.045 m
Ultimate Stress	60 N/mm^2	Displacement Limit (d_3)	0.045 m
Ultimate Strain	400%	Effective Length (L_1)	0.1 m
Viscous Damping (γ = 100%)	22 (%)	Effective Length (L_2)	1.0 m
Elastic/Post-Elastic Stiffness Ratio	13	Effective Length (L_3)	1.0 m

Inspired by FEMA P-751 section 12 [42], a set of seven ground motion records which suit the site hazard conditions were selected from the FEMA P-695 database [35] and used in the design process. Calculating the Square Root of Sum of the Squares (SRSS) and computing the average spectrum, the pseudo acceleration spectra of the ground motion records, the ASCE 7-2016 risk-targeted design spectrum, MCR_R and the scaled spectrum are illustrated in Figure 5.

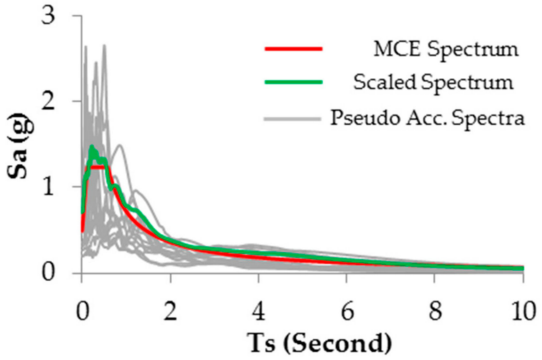

Figure 5. Design acceleration spectra. MCE: Maximum Considered Earthquake.

2.3. Numerical Models for the Performance Evaluation

A Finite Element (FE) code was developed in the OpenSees platform [47] to numerically simulate the 3D buildings. Effect of nonlinearity in both material and geometry were included in the FE code. Geometry and material nonlinearity were implemented by using P-Delta transformation and simulating plastic hinges at the ends of each beam-column element, respectively. Modified Ibarra–Medina–Krawinkler deterioration regime with bilinear hysteresis response was assigned to the plastic hinges [48]. Although the seismic isolation can decrease the superstructural nonlinearity, the behavior of panel zones was already taken into the account. The panel zones including a scissor model with nonlinear backbone curve were simulated as demonstrated in Figure 6a. Using rigid

elements to simulate the actual size of the panel and introducing a trilinear behavior for rotational springs, the corresponding force-deformation is illustrated in Figure 6b using Equations (4)–(7) [49].

$$\gamma_y = \frac{F_y}{\sqrt{3}G} \tag{4}$$

$$\gamma_p = 4\gamma_y \tag{5}$$

$$V_y = 0.55F_y.d_c.t \tag{6}$$

$$V_p = V_y(1 + \frac{3b_c t^2{}_{cf}}{d_b d_c t}) \tag{7}$$

where d_b and d_c are demonstrated in Figure 6a, F_y is the yield strength, G is shear modulus, t_{cf} is the column flange thickness, and t is thickness of panel zone which corresponds to the column.

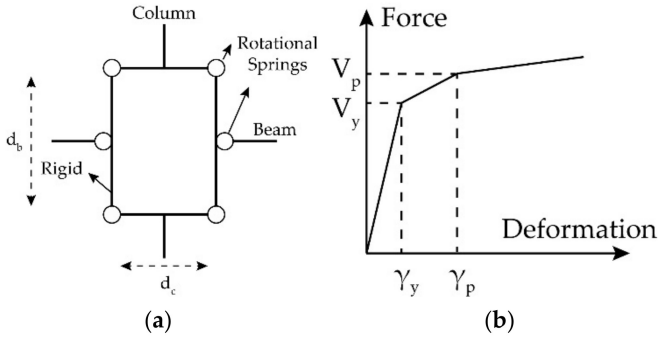

Figure 6. (**a**) The model of the panel zone [26, 49], (**b**) force-deformation backbone curve [49].

Rayleigh damping does not properly simulate the frequency content of isolated systems and results in excessive damping forces, stiffness-proportional damping with 1% ratio [50,51] was applied to the superstructural elements. The "KikuchiBearing" element, which considers shear-axial interaction together with geometric nonlinearity, was adopted to represent the numerical behavior of the LRBs [4,52]. Appropriate shear properties were assigned using "KikuchiAikenLRB" material [47]. To simulate the TCFP isolators, "TripleFrictionPendulum" element was used [2,5,47,53], where a constant friction coefficient was applied to each sliding plate.

3. Fragility Analysis and Risk Assessment

3.1. Fragility Analysis

Fragility function represents the conditional probability of occurrence of a specific Damage State (DS). A particular fragility curve can be characterized by computing the probability of occurrence of a specific Engineering Demand Parameter (EDP) exceeding a Limit State (LS). Consequently, the relationship between the intensity measure (IM) and that specific DS can be realized. In this study, a log-normal function (Equation (8)) is assumed to represent the probabilistic distribution used to develop the fragility curves.

$$P(EDP > LS|\mathrm{IM}) = \int_0^{\mathrm{IM}} \frac{1}{x\xi_x\sqrt{2\pi}}.\exp\left[-\frac{1}{2}\left(\frac{Ln(x) - \lambda_x}{\xi_x}\right)^2\right] d(IM) \tag{8}$$

where ξ_x and λ_x are the logarithmic standard deviation and mean value of the IM which corresponds to the specific DS, respectively.

Ground motion uncertainty, caused by both insufficient databases of earthquakes and the uncertainty in the seismic mechanism, can be pronounced in isolated structures since the considerable period elongation can change the dynamic characteristics. To realistically reflect the ground motion

uncertainties, the *EDP* and IM must be carefully selected [29]. Mazza and Labernarda [54] assessed the effectiveness of different IMs used in base-isolated structures, where the most suitable IM depends on parameters such as the seismic frequency content and the period ratio. Sayani and Ryan [3] used Peak Ground Acceleration (PGA) as the IM, whereas FEMA P-695 [35], Masroor and Mosqueda [55], and Tajammolian et al. [29] adopted the spectral acceleration at T_M, S_a ($T = T_M$) as the IM. Inspired by Alembagheri and Ghaemian [56] for 3D nonlinear IDA, two horizontal components per each ground motion were scaled in each step of the analysis using S_a ($T = T_M$) as the scale factor. Within the FE code, an automatic algorithm referred to hunt and fill algorithm [34] was implemented for the IDA. In addition, peak inter-story drift ratio (PIDR), maximum story acceleration (MSA), and maximum isolations shear strain (MISS) are selected as the EDPs [27,34].

3.2. Specification of the Damage States

Drift-Sensitive Structural Components (DS-SC), Drift-Sensitive Non-Structural Components (DS-NSC), and Acceleration-Sensitive Non-Structural Components (AS-NSC) are defined as the building elements [36]. The performance objectives in terms of the DSs are categorized into Slight (DS1), Moderate (DS2), Extensive (DS3), and Collapse (DS4) states [36] (Table 3). Specification of the DSs for the LRBs largely depends on the type of material used by manufacturers [27]. Generally, LRBs are capable to withstand up to 400% MISS [15,18,27,57]. Finally, the global collapse DS of the isolated system, including the isolation devices and the superstructure, is defined as a serial system. This serial sequence is considered to have reached to the collapse DS once either the superstructure has reached the DS-SC DS4 or the isolators collapse DS, respectively.

Table 3. Structural capacity and damage state definition.

Damage State ID	DS-SC [1] (%)	DS-NSC (%)	AS-NSC (g)
Slight (DS1)	0.6	0.4	0.45
Moderate (DS2)	1.2	0.8	0.9
Extensive (DS3)	3.0	2.5	1.8
Collapse (DS4)	8.0	5.0	3.6

[1.] The values belong to low-rise archetypes. The values for mid-rise and high-rise archetypes are reduced by factors 2/3 and 1/2, respectively [36]. DS-SC: Drift-Sensitive Structural Components; DS-NSC: Drift-Sensitive Non-Structural Components; AS-NSC: Acceleration-Sensitive Non-Structural Components.

3.3. Risk Assessment Methodology

To take the RTR variability into account and neutralize the structural specific characteristics, the n–year probability of occurrence of a certain DS was calculated and denoted as "the risk of the DS". The fragility curves corresponding to the DSs were integrated over the site hazard curves using the total probability theorem. Thereby, the mean annual frequency corresponding to the specific DS (λ_{DM}) was computed following Equation (9).

$$\lambda_{DM}(y) = \int G_{DM|\mathrm{IM}}(y|\mathrm{x})\mathrm{d}\lambda_{IM}(X) \quad (9)$$

where the terms $G_{DM\,|\,\mathrm{IM}}(y\,|\,x)$ and $\mathrm{d}\lambda_{IM}(x)$ represent the complementary Cumulative Distribution Function (CDF) of the parameter "y" that is conditioned on the domain "x", and a differential fragment of mean annual frequency in the specific IM, respectively.

The site hazard curve and the T_M per each model was obtained from the USGS database [58]. Computing the 50-year probability of exceedance of a damage state to a specific building component, P_{DM} (50 yr), this paper presents a new way of looking at PBEE. The P_{DM}(50 yr) was considered to evaluate the design target of ASCE/SEI 7-2010 standard [31] in addition to the ASCE/SEI 7-2016

standard. ASCE/SEI 7-2010 aims to provide a maximum uniform risk of collapse less than 1% chance of exceedance in 50 years. The $P_{DM}(50\ yr)$ was computed using Equation (10) [59].

$$P_{DM}(50yr) = 1 - (1 - \lambda_{DM})^{50} \quad (10)$$

4. Results and Discussions

4.1. Fragility Assessment

Forty-four ground motions (22 pairs) of far-field earthquakes addressed in FEMA P-695 [35] are used to perform the IDA. The IM-EDP curves corresponding to the models #2 and #22 are illustrated in Figure 7, as two examples.

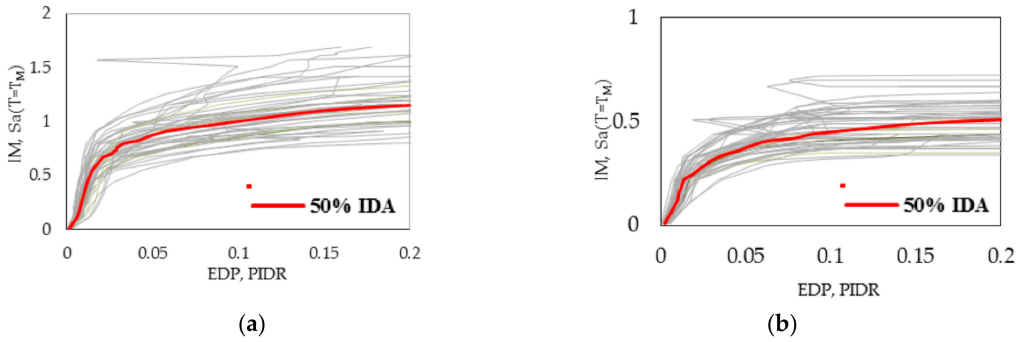

Figure 7. Incremental Dynamic Analysis (IDA) curves of archetypes (**a**) Archetype #2 (**b**) Archetype #22. IM: intensity measure; EDP: Engineering Demand Parameter; PIDR: peak inter-story drift ratio.

Since the same trend is observed among the fragility curves, selective curves related to the models #5 vs. #23, and #20 vs. #26 are illustrated in Figures 8 and 9, respectively. Among the 22 LRB isolated systems, the system collapse is mainly controlled by the failure of the isolators and rarely by the collapse of the superstructure among low-rise and mid-rise archetypes. Hence, it is recommended that each evaluated design requires detailed isolator design and an accurate representation of the isolator failure characteristics. However, for the 10-story high-rise structures with R_I = 2.0, the superstructural collapse is a dominant failure mode.

Demonstrating more dispersion, the effect of RTR variability on the AS-NSC fragility curves is more pronounced than the DS-NSC and the DS-SC fragility curves. In higher DSs, the AS-NSC fragility curves become more sensitive to the earthquake intensities and demonstrate more dispersion. However, the same trend in the dispersion of the DS-NSC, as well as DS-SC fragility curves are observed in the DSs. For instance, considering the archetype #17, the amount of Coefficient of Variation (COV) for DS-NSC and AS-NSC at DS4 is 0.19 and 0.38, respectively. Also, for the archetype #25, the amount of COV for DS-NSC and AS-NSC at DS4 is 0.2 and 0.37.

Comparing the fragility curves of AS-NSC for the TCFP and LRB isolated systems, a close performance is observed for 8-story structures in lower DSs (slight and moderate). This similarity is seen among the mid-rise archetypes having a longer effective period (T_{eff} = 3.0 s.) as well. The reason is attributed to the considerable low acceleration input. Thus, as the effective design period becomes longer and structural height becomes taller, the isolation type has less effect on the performance. Also, the LRB isolated structures having shorter design period and height (e.g., 4- story and T_D = 2.0 s) show a safer performance than their peer, TCFP isolated structures. This can be justified by severe hardening behavior of TCFPs in higher regimes. Nevertheless, the TCFP systems experience a more flexible behavior, thus superior performance to the LRB systems, in small displacement demands. Although the same trend is observed among the fragility curves of the DS-NSCs and DS-SCs, the increase in either the structural height or the effective period makes the performance of the two types of the

isolated systems closer to each other. For instance, the performance of isolated structures is virtually similar for 8-story models with T_D = 4.0 s in almost all DSs (Figure 9).

The acceptable risk per ASCE/SEI 7-16 is a probability of collapse less than 10% for regular occupancies and less than 5% for important structures given the maximum earthquake MCE. Table 1 demonstrates S_a (T = T_M) for each archetype. Evaluating the fragility curves at S_a (T = T_M), the risk of experiencing extensive and collapse damages to the high-rise archetypes with R_I = 2.0 is more than 10% (15–20% on average). Thus, the risk target of 10% in the MCE cannot always be achieved with current design procedure. Also, there is a 15–20% probability of occurrence of the extensive damage to the nonstructural components. The probability of occurrence of the moderate DS is high, ranging from 50% for DS-SCs and to 98% for NS-ASCs. Finally, the building components will experience a slight DS having a 95% probability of occurrence. Using the spectral acceleration corresponding to 50% probability of occurrence, the fragility curves can be used for loss assessment as well.

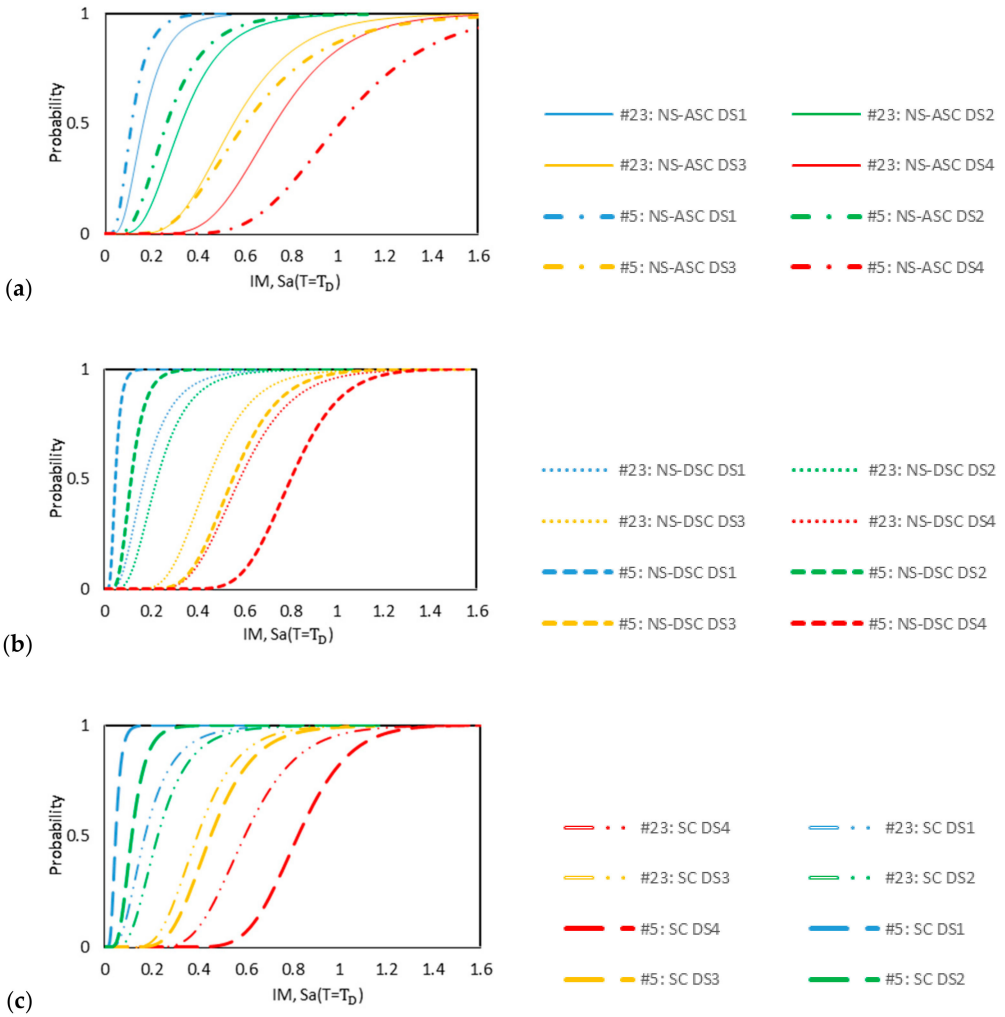

Figure 8. Fragility curves of model #5 (LRB) and model #23 (TCFP): (**a**) Acceleration-Sensitive Non-Structural Components (AS-NSC), (**b**) Drift-Sensitive Non-Structural Components (DS-NSC), (**c**) Drift-Sensitive Structural Components (DS-SC).

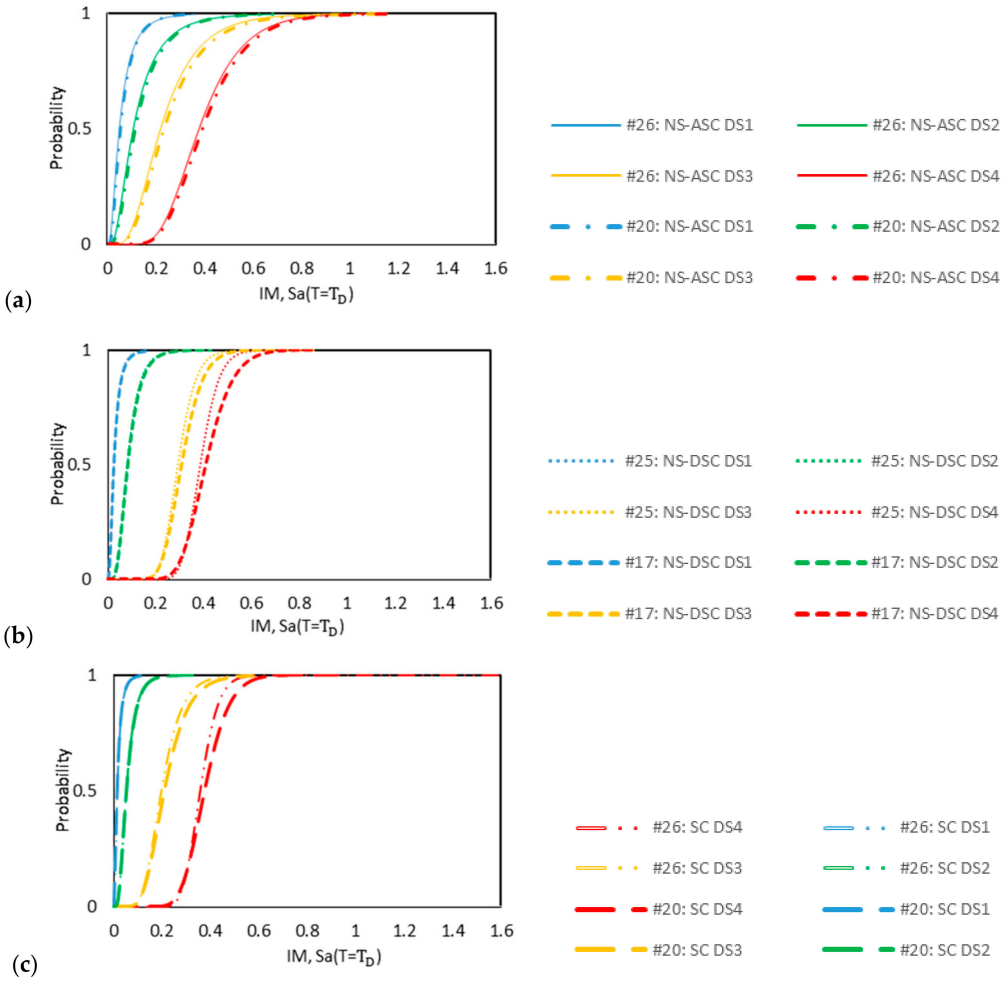

Figure 9. Fragility curves of model #20 (LRB) and model #26 (TCFP): (**a**) AS-NSC, (**b**) DS-NSC, (**c**) DS-SC.

4.2. Risk-Based Performance Assessment

The sensitivity of the seismic risk of damages to the influential parameters is established in the form of tornado diagrams. The risk of damages to the building components are calculated by integrating the fragility curves over the seismic hazard curves, which are shown in Figure 10.

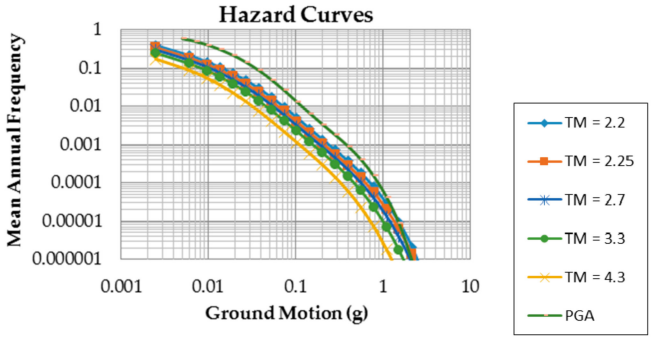

Figure 10. Seismic hazard curves of the site (The curves are provided using the USGS database [58]). PGA: Peak Ground Acceleration.

The key parameters divide the LRB isolated archetypes into three major categories. Each category has eight or nine groups, and each group contains two or three archetypes. Table 4 describes the

properties of each group. Also, Figure 11 demonstrates the legend ID of each LRB isolated model used in the risk analysis procedure.

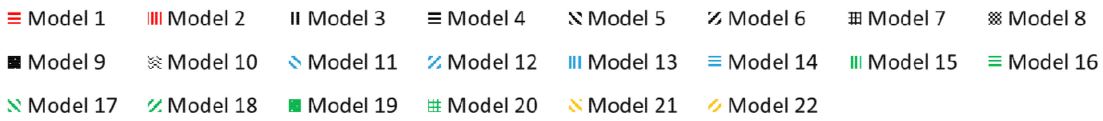

Figure 11. Identification of the LRB models for the risk assessment.

1. "Category 1": "R_I" and "T_{eff}" are constants and "height" varies from 2-story to 10-story;
2. "Category 2": "T_{eff}" and "structural height" are constants and "R_I" varies from 1.0 to 2.0;
3. "Category 3": "R_I" and "height" are constants and "T_{eff}" varies from 2.0 to 4.0 s.

Table 4. Groups and category identification.

ID	Category 1	Category 2	Category 3
Group 1	Archetypes 1, & 3	Archetypes 1, & 2	Archetypes 3, 6, & 8
Group 2	Archetypes 2, & 5	Archetypes 3, 4, & 5	Archetypes 4, & 9
Group 3	Archetypes 6, & 11	Archetypes 6, & 7	Archetypes 5, 7, & 10
Group 4	Archetypes 7, & 12	Archetypes 8, 9, & 10	Archetypes 11, & 13
Group 5	Archetypes 8, 13, & 15	Archetypes 11, & 12	Archetypes 12, & 14
Group 6	Archetypes 9, & 16	Archetypes 13, & 14	Archetypes 15, & 18
Group 7	Archetypes 10, 14, & 17	Archetypes 15, 16, & 17	Archetypes 16, & 19
Group 8	Archetypes 18, & 21	Archetypes 18, 19, & 20	Archetypes 17, & 20
Group 9	Archetypes 20, & 22	Archetypes 21, & 22	-

4.2.1. Effect of Structural Height on the Seismic Risk of Damage to the LRB Systems "Category 1"

The results demonstrate that the variation of the structural height does not lead to significant changes in the risk of damage to the AS-NSC (Figure 12). The risk of slight, moderate, extensive, and collapse damage to AS-NSC lies in the range of 25–42%, 6–12%, 1.2–2.7%, and 0.25–0.57%, respectively. Also, among the groups #3 to #9, by increasing the structural height, the risk of damage to the DS-SC as well as the DS-NSC tends to decrease per each group, especially in lower DSs.

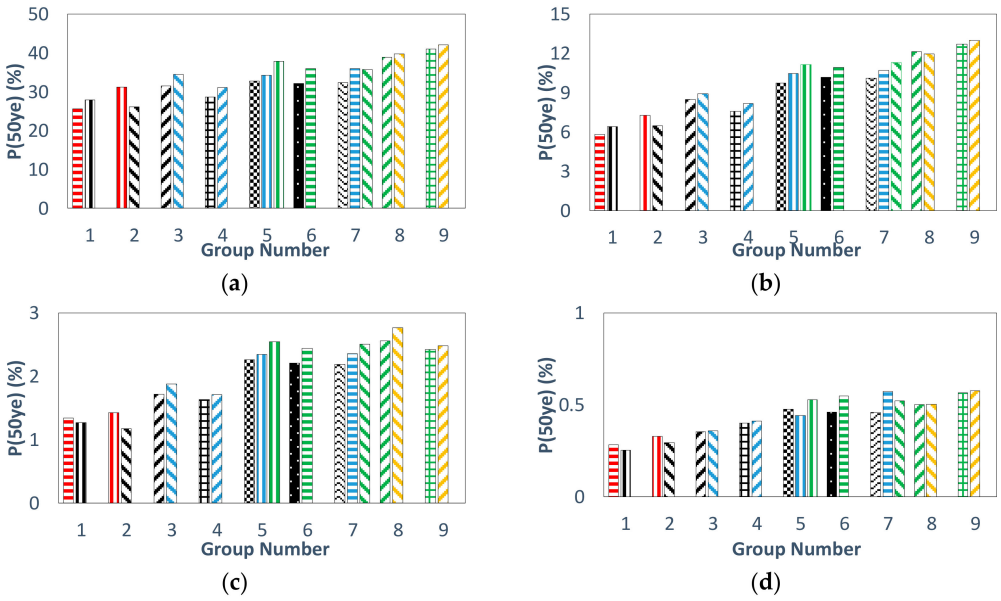

Figure 12. 50-year probability of exceedance of AS-NSC "Category 1": (**a**) DS1, (**b**) DS2, (**c**) DS3, (**d**) DS4.

Increasing the structure height from 2-story to 4-story, the risk of damage tends to increase (Figures 13 and 14). The difference in the observed trend is attributed to the difference in period-based ductility demand (μ_t), which is defined as the ratio of ultimate roof drift displacement, δ_u to the effective yield roof drift displacement, $\delta_{y,eff}$ and obtained from the nonlinear static analysis [35]. Although increasing the structural height decreases the μ_t among the groups #3 to #9, still the 4-story archetypes can provide a greater amount of μ_t than the 2-story archetypes. In fact, because of the long period transition provided by the isolators together with the low seismic input force for the 2-story models, the amount of μ_t corresponding to these archetypes is less than the other archetypes. Furthermore, the risk of damages to the DS-SC becomes less sensitive to the structural height at higher DSs (DS3 or DS4) (Figure 14). For example, the risk of slight damage occurred in the DS-SC ranges from 0.7% for 2-story archetypes to 89.7% for 10-story archetypes. However, the corresponding value for collapse DSs ranges only from 0.1% to 0.5%.

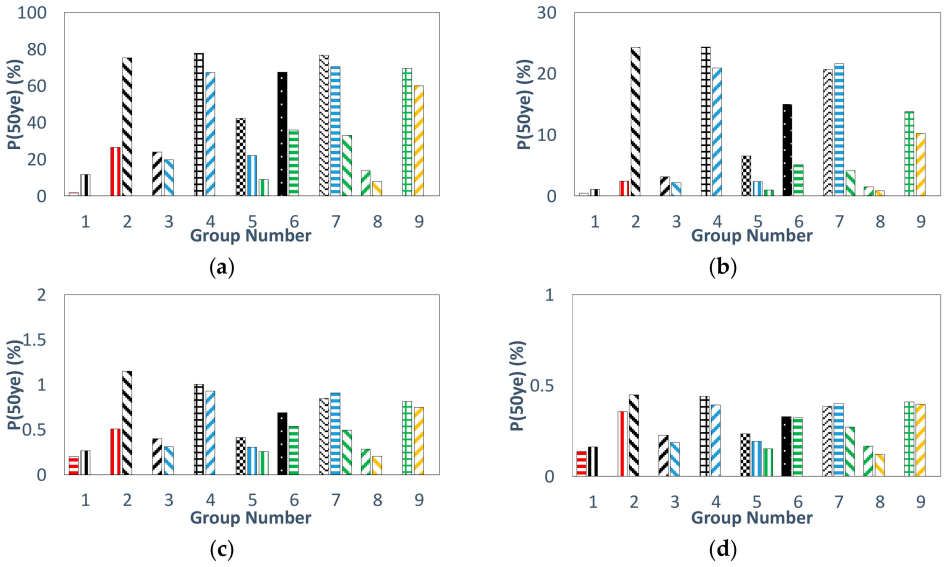

Figure 13. 50-year probability of exceedance of DS-NSC "Category 1": (**a**) DS1, (**b**) DS2, (**c**) DS3, (**d**) DS4.

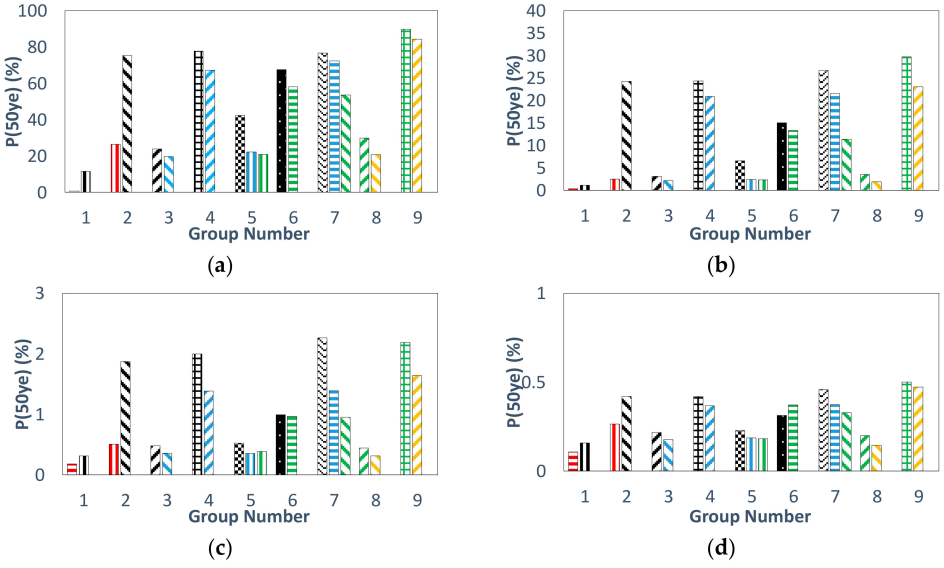

Figure 14. 50-year probability of exceedance of SC "Category 1": (**a**) DS1, (**b**) DS2, (**c**) DS3, (**d**) DS4.

Increasing the height, the seismic risk of the system collapse increases insignificantly per each group (Figure 15) and it can be concluded that it remains almost constant. However, there is a difference between the risk values of models #1 and #3 (Group 1). In fact, model #1 meets the system collapse limit state by having the failure in its LRBs. This is because of the short structural height and low response modification factor for the superstructure (R_I = 1.0). Contrarily, its 4-story peer (model #3) experiences the system collapse by meeting the superstructural collapse criteria. Therefore, the risk of the system collapse for this group is different from the trend observed in the rest. The average value for risk of collapse is approximately 0.38%.

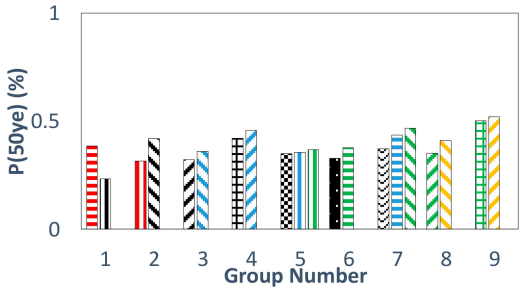

Figure 15. 50-year probability of exceedance of isolated system collapse "Category 1".

4.2.2. Effect of R_I on the Seismic Risk of Damage to the LRB Systems "Category 2"

Changes in the R_I do not affect the seismic risk of damages to AS-NSC per each group, and they remain almost constant over the DSs (Figure 16). Also, among the DS-NSC, the archetypes with greater R_I are more vulnerable than those with smaller R_I, indicating the importance of superstructure behavior itself along with the isolator characteristics. On average, increasing the R_I from 1.0 to 2.0, 45%, 13.7%, 0.53%, and 0.22% are added to the risk values associated with DS1, DS2, DS3, and DS4, respectively (Figure 17). Similarly, among the DS-SC, the archetypes with greater R_I are more vulnerable than the other archetypes. Also, lower DSs are more sensitive to the changes of R_I. On average, by increasing the R_I from 1.0 to 2.0, 48.05%, 16.9%, 1.03%, and 0.21% will be added to the average risk of damage associated with the DS1, DS2, DS3, and DS4, respectively (Figure 18).

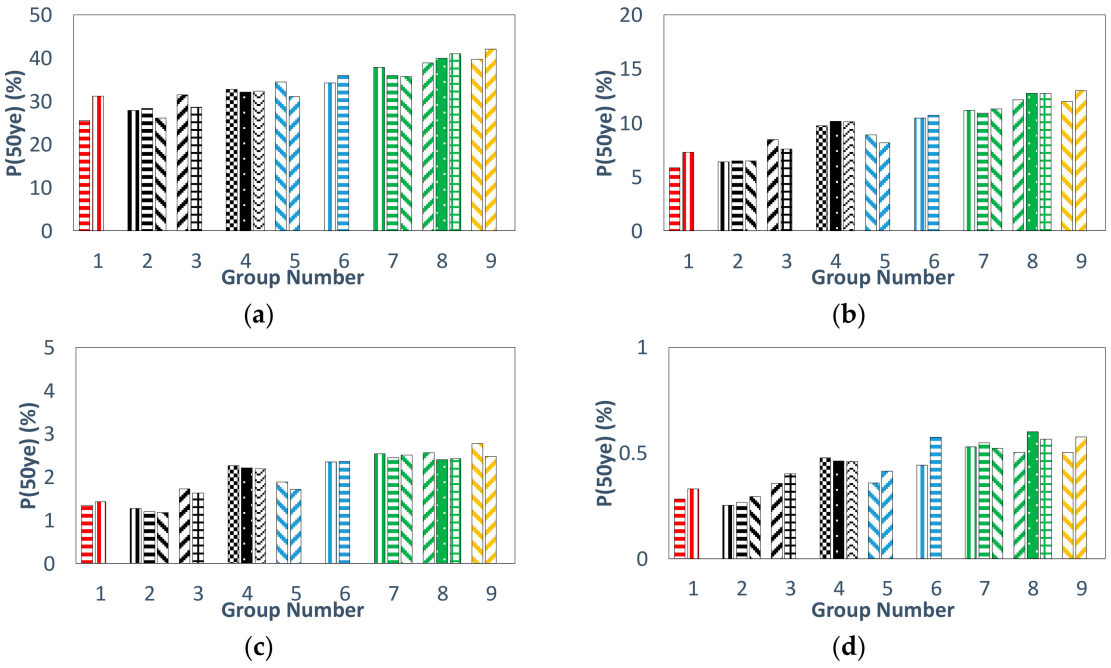

Figure 16. 50-year probability of exceedance of AS-NSC "Category 2": (**a**) DS1, (**b**) DS2, (**c**) DS3, (**d**) DS4.

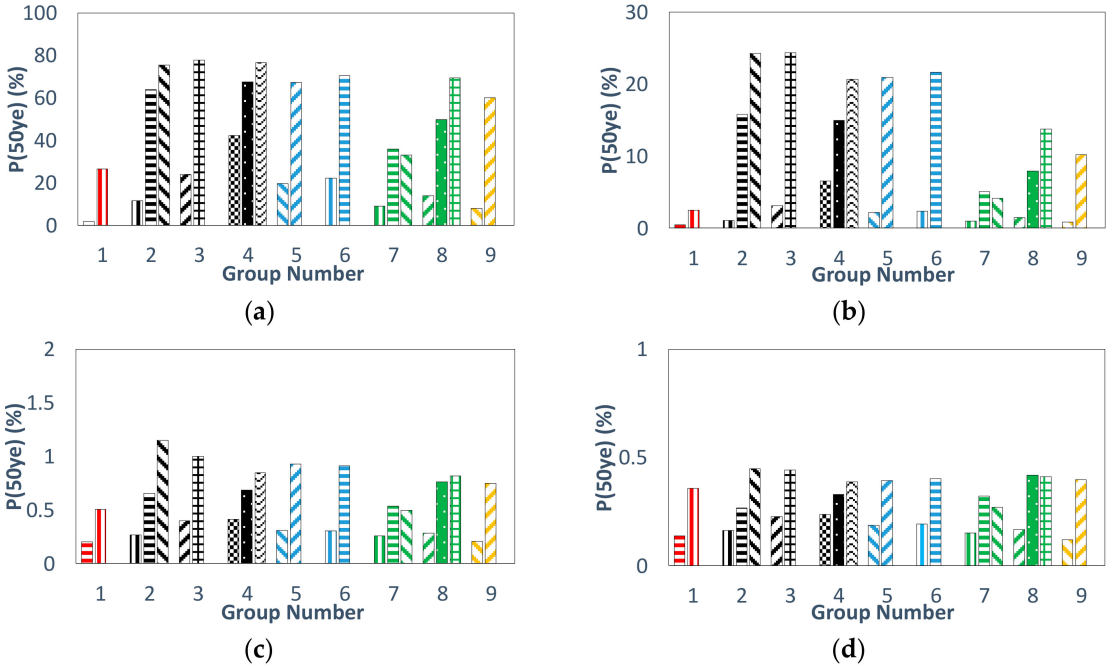

Figure 17. 50-year probability of exceedance of DS-NSC "Category 2": (**a**) DS1, (**b**) DS2, (**c**) DS3, (**d**) DS4.

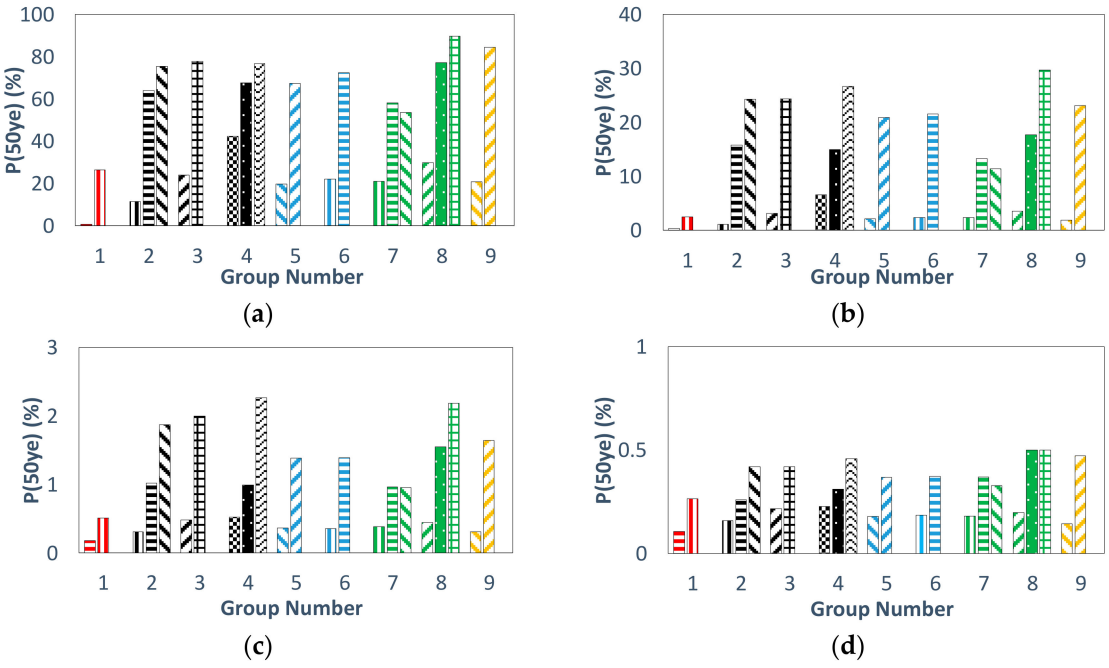

Figure 18. 50-year probability of exceedance of SC "Category 2": (a) DS1, (b) DS2, (c) DS3, (d) DS4.

Variations in the R_I lead to minor changes in the seismic risk of damage associated with the isolation system collapse. Figure 19 shows the associated 50-year probability of exceedance. This insignificant change is because of the effects of the transformed period which reduce the earthquake seismic input to the superstructure. However, among the archetypes, 4-story buildings with T_D = 2.0 s are more sensitive to the variations of the R_I. This could be attributed to the fact that the T_{eff} = 2.0 s might not be capable enough to reduce the seismic input forces, as efficient as other effective periods (Figure 19). The risk of collapse ranges from 0.23% for the archetype #3 to 0.52% for the archetype #22.

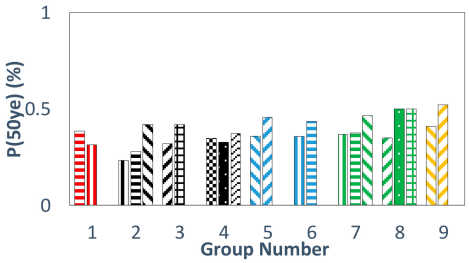

Figure 19. 50-year probability of exceedance of isolated system collapse "Category 2".

4.2.3. Effect of T_{eff} on the Seismic Risk of Damage to the LRB Systems "Category 3"

Making the T_{eff} longer, the seismic risk of damage to the AS-NSC increases slightly in the mid-rise archetypes. However, in the high-rise archetypes, the associated risk of damage remains almost unchanged in all DSs (Figure 20). This shows that the variations in T_{eff} do not affect the risk of damage to the AS-NSC among the high-rise buildings.

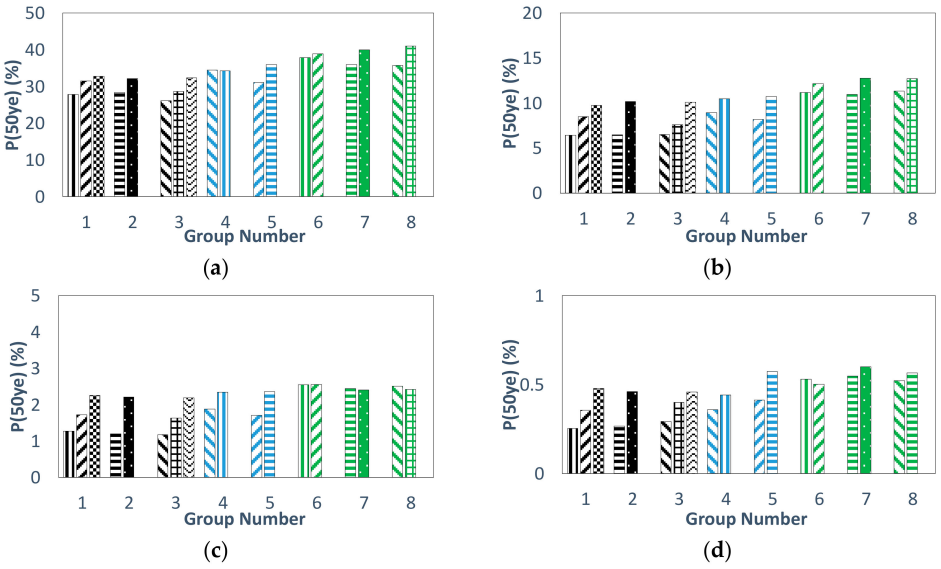

Figure 20. 50-year probability of exceedance of AS-NSC "Category 3": (**a**) DS1, (**b**) DS2, (**c**) DS3, (**d**) DS4.

The changes in T_{eff} do not significantly affect the risk of damage to the DS-NSC (Figure 21) and DS-SC (Figure 22), except the groups #1, #7, and #8, where the risk of damage is increased by having a longer T_{eff}, especially in lower DSs. In fact, a longer T_{eff} can potentially reduce the seismic design load. Consequently, the section size of superstructures becomes smaller and it is more probable for the superstructure to reach to a specific DS in lower seismic intensities. In this regard, the structure which has longer a T_{eff} experiences a greater risk of damages to DS-NSC, as well as DS-SC, than the others. It is very important to mention that this increase in the risk values will happen only if the T_D controls the seismic design force. In other words, the amount of design force (Equation (11)), must exceed the design requirements per Section 17.5.4.3 of the ASCE/SEI 7-2016. Otherwise, any change in the T_D does not cause significant variations in the seismic risk of damage.

$$V_S = \frac{K_D.D_D}{R_I} \tag{11}$$

where K_D, D_D, and R_I are the effective stiffness at design displacements, isolation displacement at the design level, and isolated response modification factor, respectively.

In fact, Section 17.5.4.3 of the ASCE 7-2016 provides some constraints for the design force in order to fully activate the isolation system at the design level. The design forces should not be taken as less than:

1. "The lateral seismic force required for a fixed-base structure of the same effective seismic weight, and a period equal to the period of the isolation system using the upper bound properties T_M ";
2. "The base shear corresponding to the factored design wind load";
3. The lateral seismic force required to fully activate the system using the upper bound properties of the isolation system

By that means, the design force can be controlled by defining the minimum required amounts. Consequently, a uniform risk stage among archetypes with different effective periods can be induced. Because the seismic force calculated from Section 17.5.4.3 dominates the seismic force resulting from Equation (11), no significant changes occur among risk of damage associated with the groups 2 to 6. Finally, regarding the collapse assessment, the isolated structures are less sensitive to the variations of the T_{eff} at the collapse DS (Figure 23).

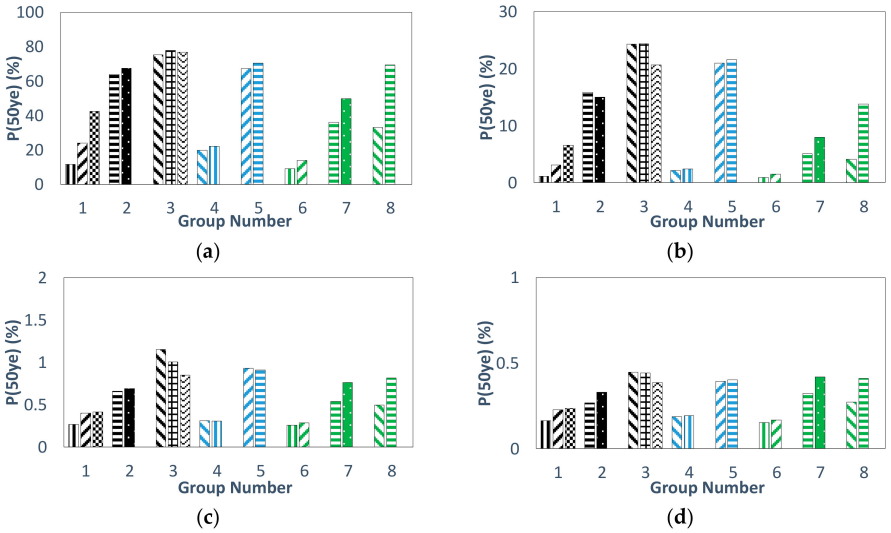

Figure 21. 50-year probability of exceedance of DS-NSC "Category 3": (**a**) DS1, (**b**) DS2, (**c**) DS3, (**d**) DS4.

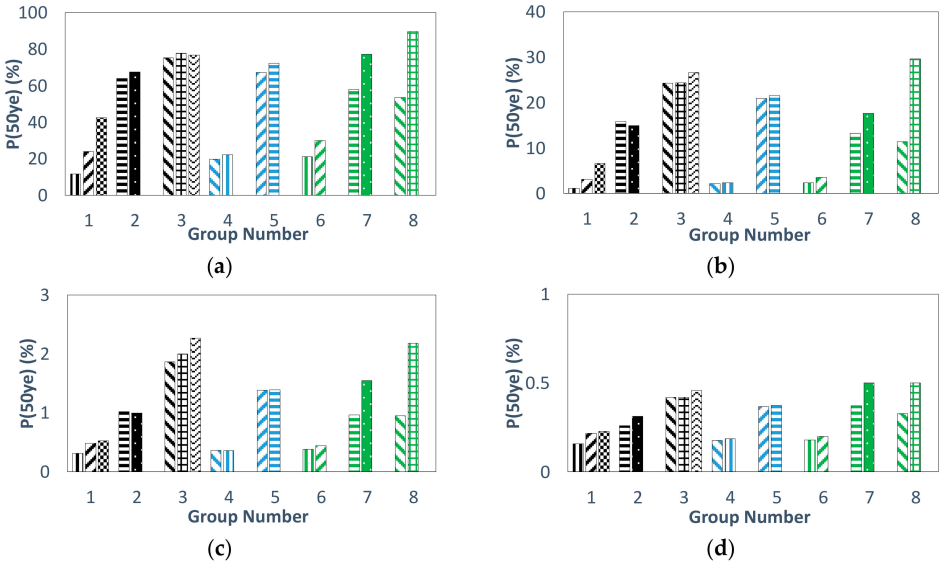

Figure 22. 50-year probability of exceedance of DS-SC "Category 3": (**a**) DS1, (**b**) DS2, (**c**) DS3, (**d**) DS4.

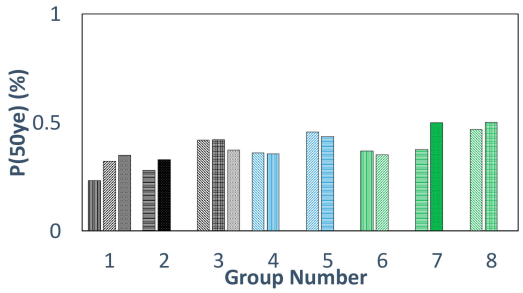

Figure 23. 50-year probability of exceedance of isolated system collapse "Category 3".

4.2.4. Effect of the Isolation Type on the Seismic Performance

Seismic risk of damage for structural and non-structural components for the TCFP isolated structures is calculated and compared to their peers, LRB isolated systems, at the collapse DS (Figure 24). Among the AS-NSC, changing the isolation system from LRB to TCFP affects the risk of collapse among the mid-rise archetypes, while the changes among the high-rise structures are almost negligible. Generally, the models equipped with the LRB isolators have a less seismic risk of damage than TCFP isolated systems. Furthermore, the selection of isolation type affects the seismic risk of damage to DS-NSC for mid-rise buildings more than the other cases. Changing the system from LRB to TCFP increases the seismic risk of collapse damage. However, changing the isolation system does not affect the seismic risk of collapse of high-rise structures, especially those that have longer effective periods. Furthermore, implementing the TCFP isolators instead of LRB isolators can raise the seismic risk of damage to the DS-SC, especially among 8-story structures. On average, a 41% and 85% increase are observed in the risk values corresponding to the collapse DS of 4-story and 8-story structures, respectively. Finally, the seismic risk of collapse damage for TCFP isolated models, which are designed per the ASCE 7-2016, are derived less than, but near to 1% in 50 years.

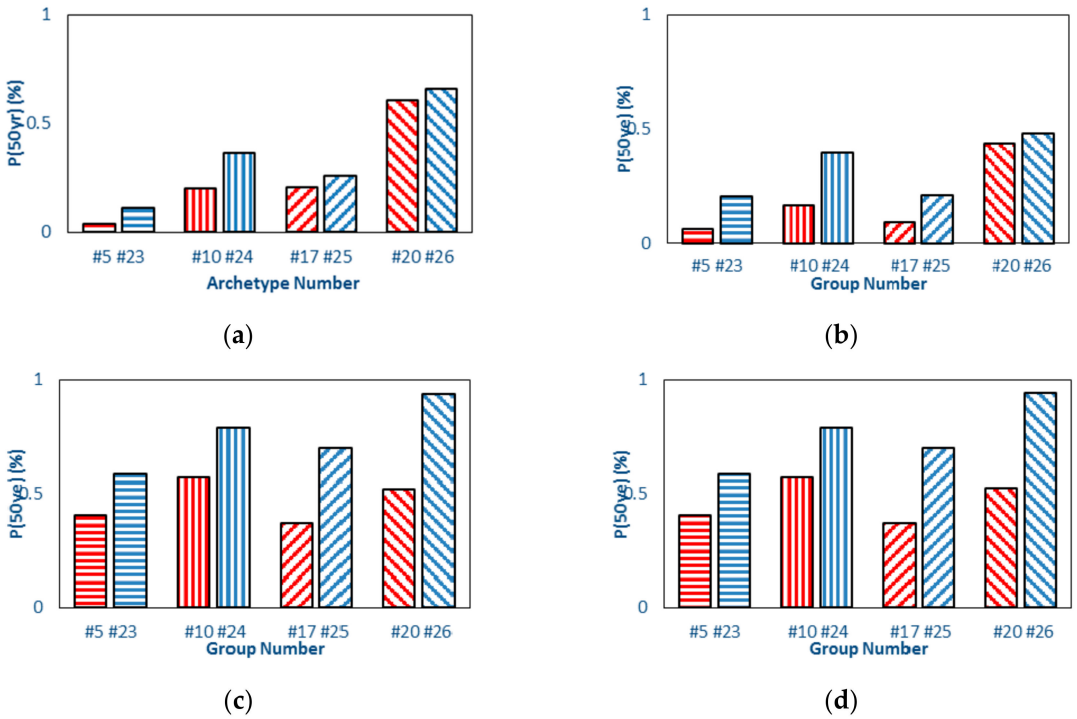

Figure 24. The 50-year probability of exceedance of (**a**)AS-NSC, (**b**) DS-NSC, (**c**) DS-SC, and (**d**) isolation system collapse for TCFP and LRB systems.

5. Conclusions

Conforming to the PBEE methodology, the seismic risk-based performance assessment of base-isolated steel structures was conducted in this study. The special moment resisting frames were designed per the ASCE/SEI 7-2016 standard. Twenty-six archetypes mounting on LRB and TCFP isolation devices are simulated in the OpenSees platform using nonlinear 3D Finite Element Method. Ground motion uncertainty was taken into account through nonlinear incremental dynamic analyses. The fragility curves corresponding to slight, moderate, extensive, and collapse damage to the structural, as well as non-structural (both drift- and acceleration-sensitive), components were provided. As such, the performance of the building components were assessed. Afterward, following the risk evaluation method using the total probability theorem, 50-year probability of exceedance was computed per each damage state per building components. Finally, a sensitivity analysis was applied to assess the effect of structural height, the effective transformed period of the isolated structure (T_{eff}), the isolated response modification factor (R_I), and the isolation type on the seismic risk of damages to the archetypes.

Generally, the record-to-record variability has a significant effect on the AS-NSC fragility curves. Also, for higher damage states, the fragility curves of AS-NSC become more sensitive to the ground motion intensities. Furthermore, the dispersion of the fragility curves corresponding to the either DS-NSC or DS-SC is virtually the same in whole DSs. It is concluded that as the effective design period becomes longer and structural height becomes taller, the isolation type has less effect on the performance of non-structural components. Comparing the TCFP and LRB isolated archetypes through the fragility curves, a safer performance of TCFP isolated systems in lower intensities which impose slight and moderate damage states is observed. In contrast, the LRB isolated structures demonstrate safer performance in higher shocks which cause severe damage states. Furthermore, among the archetypes having shorter effective periods and heights, the LRB isolated structures show a safer performance than the TCFP ones. Moreover, evaluating the performance of the archetypes at the MCE level, the risk of experiencing extensive and collapse damages for the high-rise archetypes with $R_I = 2.0$ is more than 10%, which does not satisfy the current design target per ASCE/SEI 7-2016. Also, slight damage state can occur with more than 95% probability of occurrence. As addressed in Reference [57], providing sufficient restoring force is essential to guarantee the continuous functionality of isolation devices. Comparing the fragility curves, it is concluded that both isolation types are able to satisfy this performance objective in lower intensities which correspond to light and moderate damage state. For intense ground motions, TCFPs demonstrate superior performance.

Through the risk assessment procedure, the variation of structural height does not lead to a significant change in the risk of damage to the AS-NSC. Also, changes in the R_I do not affect the seismic risk values of the AS-NSC. By making the T_{eff} longer, the seismic risk of damage to AS-NSC increases slightly in the mid-rise archetypes but remains constant among the high-rise structures. In cases where period-based ductility demand becomes less, by increasing the structural height, the risk of damage to the DS-SC and DS-NSC tends to decrease. Changes in T_{eff} do not change the risk of damage to DS-SC and DS-NSC only if the T_{eff} controls the seismic design force of the superstructure. Also, the drift-sensitive components of the archetypes having a greater R_I are more vulnerable than those with smaller R_I. Also, by increasing the height, the seismic risk of collapse damage state increases insignificantly (almost constant). This indicates that the isolation technique may not be an optimized strategy to control high-rise structures. Variations in the R_I lead to minor changes (increases) in the seismic risk of damage associated with the isolation system collapse. Isolated structures are not sensitive to the variations of the T_{eff} in system collapse DSs. Changing the isolation system from LRB to TCFP increases the risk of the system collapse among the mid-rise archetypes, while changes among the high-rise structures are almost negligible. Implementing the TCFP isolators instead of LRB isolators can raise the seismic risk of collapse damage state for DS-SC. The risk of the system collapse among the codified archetypes were less than 1% in 50 years, which confirms the ASCE/SEI 7-2010 "risk-targeted" design approach.

The performance was looked at not only in terms of collapse but also in terms of other parameters that denote potential for damage to the structural and non-structural components and contents. To accomplish the functionality criteria, it is recommended to adopt an essentially elastic design (R = 1 in the DBE), stiff structural system (drift less than about 0.3%), limited floor spectra acceleration to 0.4 g, and large displacement capacity isolators with displacement capacity about 75% more than the average in the MCE (and much larger when the isolators lack stiffening behavior). Finally, modeling uncertainty can be included in further performance assessments. Parameters such as the initial and post-elastic stiffness, characteristic strength, and the temperature can be affected by the modeling uncertainty and treated as random variables in addition to the RTR uncertainty. Since the distribution of the mechanical characteristics depends on the manufacturer, a uniform distribution function is recommended [27].

Author Contributions: Investigation and writing were carried out by the authors, Aryan Rezaei Rad and Mehdi Banazadeh. Numerical modelings, validation and data post-processing were carried out by Aryan Rezaei Rad. Supervision, review and editions were done by Mehdi Banazadeh at Amirkabir University of Technology (Tehran Polytechnic).

Funding: This research article was a part of a M.Sc. thesis and received no external funding.

Conflicts of Interest: The authors declare no conflict of interest.

References

1. N aeim, F.; Kelly, J.M. *Design of Seismic Isolated Structures: From Theory to Practice*; John Wiley & Sons: New York, NY, USA, 1999; ISBN 0-471-14921-7.
2. Erduran, E.; Dao, N.D.; Ryan, K.L. Comparative response assessment of minimally compliant low-rise conventional and base-isolated steel frames. *Earthq. Eng. Struct. Dyn.* **2011**, *40*, 1123–1141. [CrossRef]
3. Sayani, P.J.; Ryan, K.L. Comparative Evaluation of Base-Isolated and Fixed-Base Buildings Using a Comprehensive Response Index. *J. Struct. Eng.* **2009**, *135*, 698–707. [CrossRef]
4. Kikuchi, M.; Nakamura, T.; Aiken, I.D. Three-dimensional analysis for square seismic isolation bearings under large shear deformations and high axial loads. *Earthq. Eng. Struct. Dyn.* **2010**, *39*, 1513–1531. [CrossRef]
5. Fenz, D.M.; Constantinou, M.C. Modeling Triple Friction Pendulum Bearings for Response-History Analysis. *Earthq. Spectra* **2008**, *24*, 1011–1028. [CrossRef]
6. Becker, T.C.; Mahin, S.A. Experimental and analytical study of the bi-directional behavior of the triple friction pendulum isolator. *Earthq. Eng. Struct. Dyn.* **2012**, *41*, 355–373. [CrossRef]
7. Becker, T.C.; Bao, Y.; Mahin, S.A. Extreme behavior in a triple friction pendulum isolated frame. *Earthq. Eng. Struct. Dyn.* **2017**, *46*, 2683–2698. [CrossRef]
8. Sarlis, A.A.; Constantinou, M.C. A model of triple friction pendulum bearing for general geometric and frictional parameters. *Earthq. Eng. Struct. Dyn.* **2016**, *45*, 1837–1853. [CrossRef]
9. Fenz, D.M.; Constantinou, M.C. Spherical sliding isolation bearings with adaptive behavior: Theory. *Earthq. Eng. Struct. Dyn.* **2008**, *37*, 163–183. [CrossRef]
10. Azimi, M. *Design of Structural Vibration Control Using Smart Materials and Devices for Earthquake-Resistant and Resilient Buildings*; North Dakota State University: Fargo, ND, USA, 2017.
11. Ozbulut, O.E.; Hurlebaus, S. Seismic Protection of Bridge Structures Using Shape Memory Alloy-Based Isolation Devices. In Proceedings of the Structures Congress 2011; American Society of Civil Engineers: Reston, VA, USA, 2011; pp. 2066–2077.
12. Ozbulut, O.E.; Hurlebaus, S. Seismic assessment of bridge structures isolated by a shape memory alloy/rubber-based isolation system. *Smart Mater. Struct.* **2011**, *20*, 015003. [CrossRef]
13. Yenidogan, C.; Erdik, M. A comparative evaluation of design provisions for seismically isolated buildings. *Soil Dyn. Earthq. Eng.* **2016**, *90*, 265–286. [CrossRef]
14. Shahir, H.; Pak, A.; Ayoubi, P. A performance-based approach for design of ground densification to mitigate liquefaction. *Soil Dyn. Earthq. Eng.* **2016**, *90*, 381–394. [CrossRef]
15. Siqueira, G.H.; Sanda, A.S.; Paultre, P.; Padgett, J.E. Fragility curves for isolated bridges in eastern Canada using experimental results. *Eng. Struct.* **2014**, *74*, 311–324. [CrossRef]

16. Karim, K.R.; Yamazaki, F. Effect of isolation on fragility curves of highway bridges based on simplified approach. *Soil Dyn. Earthq. Eng.* **2007**, *27*, 414–426. [CrossRef]
17. Mohebbi, A.; Ryan, K.L.; Sanders, D.H. Seismic Protection of the Piers of Integral Bridges using Sliding Bearings. *J. Earthq. Eng.* **2017**, *21*, 1365–1384. [CrossRef]
18. Zhang, J.; Huo, Y. Evaluating effectiveness and optimum design of isolation devices for highway bridges using the fragility function method. *Eng. Struct.* **2009**, *31*, 1648–1660. [CrossRef]
19. Dao, N.D.; Ryan, K.L. Computational simulation of a full-scale, fixed-base, and isolated-base steel moment frame building tested at E-defense. *J. Struct. Eng.* **2014**, *140*. [CrossRef]
20. Chimamphant, S.; Kasai, K. Comparative response and performance of base-isolated and fixed-base structures. *Earthq. Eng. Struct. Dyn.* **2016**, *45*, 5–27. [CrossRef]
21. Morgan, T.A.; Mahin, S.A. Achieving reliable seismic performance enhancement using multi-stage friction pendulum isolators. *Earthq. Eng. Struct. Dyn.* **2010**, *39*, 1443–1461. [CrossRef]
22. Castaldo, P.; Amendola, G.; Palazzo, B. Seismic fragility and reliability of structures isolated by friction pendulum devices: Seismic reliability-based design (SRBD). *Earthq. Eng. Struct. Dyn.* **2017**, *46*, 425–446. [CrossRef]
23. Applied Technology Council. *FEMA P-58: Seismic Performance Assessment of Buildings*; FEMA: Redwood City, CA, USA, 2012.
24. Lee, H.-P.; Kim, S.; Cho, M.-S.; Ji, Y.-S. Application of sliding seismic isolator to building structures considering cost, performance and inspection: A case study. *Struct. Infrastruct. Eng.* **2015**, *11*, 851–868. [CrossRef]
25. Banazadeh, M.; Gholhaki, M.; Parvini Sani, H. Cost-benefit analysis of seismic-isolated structures with viscous damper based on loss estimation. *Struct. Infrastruct. Eng.* **2016**, *2479*. [CrossRef]
26. Parvini Sani, H.; Gholhaki, M.; Banazadeh, M. Simplified direct loss measure for seismic isolated steel moment-resisting structures. *J. Constr. Steel Res.* **2018**, *147*, 313–323. [CrossRef]
27. Han, R.; Li, Y.; van de Lindt, J. Seismic risk of base isolated non-ductile reinforced concrete buildings considering uncertainties and mainshock–aftershock sequences. *Struct. Saf.* **2014**, *50*, 39–56. [CrossRef]
28. Cutfield, M.; Ryan, K.; Ma, Q. Comparative life cycle analysis of conventional and base-isolated buildings. *Earthq. Spectra* **2016**, *32*, 323–343. [CrossRef]
29. Tajammolian, H.; Khoshnoudian, F.; Rezaei Rad, A.; Loghman, V. Seismic Fragility Assessment of Asymmetric Structures Supported on TCFP Bearings Subjected to Near-field Earthquakes. *Structures* **2018**, *13*, 66–78. [CrossRef]
30. Almufti, I.; Willford, M. The REDi^{TM} rating system: A framework to implement resilience-based earthquake design for new buildings. In Proceedings of the NCEE 2014—10th U.S. National Conference on Earthquake Engineering: Frontiers of Earthquake Engineering, Anchorage, AL, USA, 21–25 July 2014.
31. American Society of Civil Engineers. *ASCE/SEI 7-2010 Minimum Design Loads for Buildings and Other Structures*; American Society of Civil Engineers: Reston, VA, USA, 2013.
32. American Society of Civil Engineers. *ASCE/SEI 7-2016 Minimum Design Loads and Associated Criteria for Buildings and Other Structures*; American Society of Civil Engineers: Reston, VA, USA, 2016.
33. Tubaldi, E.; Mitoulis, S.A.; Ahmadi, H. Comparison of different models for high damping rubber bearings in seismically isolated bridges. *Soil Dyn. Earthq. Eng.* **2018**, *104*, 329–345. [CrossRef]
34. Vamvatsikos, D.; Cornell, C.A. Incremental dynamic analysis. *Earthq. Eng. Struct. Dyn.* **2002**, *31*, 491–514. [CrossRef]
35. Applied Technology Council. *FEMA P-695: Quantification of Building Seismic Performance Factors*; FEMA: Redwood City, CA, USA, 2009.
36. *HAZUS®-MH 2.1: Multi-Hazard Loss Estimation Methodology Earthquake Model*; National Institute of Building Sciences: Washington, DC, USA, 2009.
37. Ayoubi, P.; Pak, A. Liquefaction-induced settlement of shallow foundations on two-layered subsoil strata. *Soil Dyn. Earthq. Eng.* **2017**, *94*, 35–46. [CrossRef]
38. USGS Urban Seismic Hazard Maps. Available online: https://earthquake.usgs.gov/hazards/urban/ (accessed on 12 July 2018).
39. Bridgestone Corporation, Seismic isolation product line-up, Seismic Isolation & Vibration Control Products Business Department. 2017. Available online: http://www.bridgestone.com/products/diversified/antiseismic_rubber/index.html (accessed on 16 June 2018).

40. Applied Technology Council. *FEMA P-1050: NEHRP Recommended Seismic Provisions for New Buildings and Other Structures*; FEMA: Redwood City, CA, USA, 2015.
41. Applied Technology Council. *FEMA P-750: NEHRP Recommended Seismic Provisions for New Buildings and Other Structures*; FEMA: Redwood City, CA, USA, 2009.
42. Applied Technology Council. *FEMA P-751: 2009 NEHRP Recommended Seismic Provisions: Design Examples*; FEMA: Redwood City, CA, USA, 2009.
43. *ANSI/AISC 360-10 Specification for Structural Steel Buildings*; American Institute of Steel Construction: Chicago, IL, USA, 2010.
44. *ANSI/AISC 341-10 Seismic Provisions for Structural Steel Buildings*; American Institute of Steel Construction: Chicago, IL, USA, 2010.
45. AISC Steel Shape Database. Available online: https://www.aisc.org/search/?query=shapesdatabase&pageSize=10&page=1 (accessed on 10 July 2018).
46. Constantinou, M.C.; Kalpakidis, I.; Filiatrault, A.; Ecker Lay, R.A. *LRFD-Based Analysis and Design Procedures for Bridge Bearings and Seismic Isolators: MCEER-11-0004*; MCEER: Buffalo, NY, USA, 2011.
47. McKenna, F. OpenSees: A Framework for Earthquake Engineering Simulation. *Comput. Sci. Eng.* **2011**, *13*, 58–66. [CrossRef]
48. Lignos, D.G.; Krawinkler, H. Deterioration Modeling of Steel Components in Support of Collapse Prediction of Steel Moment Frames under Earthquake Loading. *J. Struct. Eng.* **2011**, *137*, 1291–1302. [CrossRef]
49. Foutch, D.A.; Yun, S.-Y. Modeling of steel moment frames for seismic loads. *J. Constr. Steel Res.* **2002**, *58*, 529–564. [CrossRef]
50. Ryan, K.L.; Polanco, J. Problems with Rayleigh Damping in Base-Isolated Buildings. *J. Struct. Eng.* **2008**, *134*, 1780–1784. [CrossRef]
51. Pant, D.R.; Wijeyewickrema, A.C.; ElGawady, M.A. Appropriate viscous damping for nonlinear time-history analysis of base-isolated reinforced concrete buildings. *Earthq. Eng. Struct. Dyn.* **2013**, *42*, 2321–2339. [CrossRef]
52. Yamamoto, S.; Kikuchi, M.; Ueda, M.; Aiken, I.D. A mechanical model for elastomeric seismic isolation bearings including the influence of axial load. *Earthq. Eng. Struct. Dyn.* **2009**, *38*, 157–180. [CrossRef]
53. Dao, N.D.; Ryan, K.L.; Sato, E.; Sasaki, T. Predicting the displacement of triple pendulum^{TM} bearings in a full-scale shaking experiment using a three-dimensional element. *Earthq. Eng. Struct. Dyn.* **2013**, *42*, 1677–1695. [CrossRef]
54. Mazza, F.; Labernarda, R. Structural and non-structural intensity measures for the assessment of base-isolated structures subjected to pulse-like near-fault earthquakes. *Soil Dyn. Earthq. Eng.* **2017**, *96*, 115–127. [CrossRef]
55. Masroor, A.; Mosqueda, G. Assessing the Collapse Probability of Base-Isolated Buildings Considering Pounding to Moat Walls Using the FEMA P695 Methodology. *Earthq. Spectra* **2015**, *31*, 2069–2086. [CrossRef]
56. Alembagheri, M.; Ghaemian, M. Damage assessment of a concrete arch dam through nonlinear incremental dynamic analysis. *Soil Dyn. Earthq. Eng.* **2013**, *44*, 127–137. [CrossRef]
57. Monzon, E.V.; Buckle, I.G.; Itani, A.M. Seismic Performance and Response of Seismically Isolated Curved Steel I-Girder Bridge. *J. Struct. Eng.* **2016**, *142*, 04016121. [CrossRef]
58. United States Geological Survey (USGS) Unified Hazard Tool. Available online: https://earthquake.usgs.gov/hazards/interactive/ (accessed on 28 February 2018).
59. Frangopol, D.M. *Probability Concepts in Engineering: Emphasis on Applications to Civil and Environmental Engineering*; Taylor & Francis: London, UK, 2008.